

Modeling individual nearby radio galaxies as ultra-high-energy cosmic-ray accelerators

Andressa Colaço,^a Gabriel Azeredo,^a Isadora Parillo,^a Cainã de Oliveira,^b and Vitor de Souza^a

^aInstituto de Física de São Carlos, Universidade de São Paulo,
Av. Trabalhador São Carlense, 400, São Carlos, SP, 13566-590, Brazil

^bInstituto de Física, Universidade de São Paulo,
Rua Do Matão 1371, São Paulo, SP, 05508-090, Brazil

E-mail: andressacolaco@usp.br, gabriel@ifsc.usp.br, isadora.parillo@usp.br,
caina.oliveira@usp.br, vitor@ifsc.usp.br

Abstract. Nearby radio galaxies are among the most promising candidates for the acceleration of ultra-high-energy cosmic rays (UHECRs). In this work, we develop a physically motivated, source-resolved framework to quantify the contribution of the three nearest FR-I radio galaxies—Centaurus A, Virgo A, and Fornax A to the UHECR flux measured by the Pierre Auger Observatory. Acceleration spectra derived from detailed jet-acceleration models are combined with numerical simulations of extragalactic propagation, while the more distant radio-galaxy population is treated as a continuous background. By fitting exclusively the measured UHECR energy spectrum, we determine the relative contribution of each source and constrain the fraction of jet power converted into UHECR luminosity. We find that a small number of nearby radio galaxies can account for the highest-energy UHECR flux with acceleration efficiencies of order 10^{-3} – 10^{-2} , while the background contribution remains subdominant. The resulting scenarios yield mass-composition trends broadly consistent with observations and predict distinct levels of secondary neutrino fluxes. These results demonstrate that physically grounded, source-specific modeling of nearby radio galaxies provides a viable and predictive explanation for the origin of the highest-energy cosmic rays.

Contents

| | | |
|----------|--|-----------|
| 1 | Introduction | 1 |
| 2 | Radio galaxies as UHECR sources | 2 |
| 2.1 | Energy spectrum and composition | 3 |
| 2.2 | Emitted Power | 4 |
| 2.3 | Sources distribution | 4 |
| 3 | Simulation setup and data analysis method | 6 |
| 3.1 | Extragalactic propagation | 6 |
| 3.2 | Procedure to fit the measured energy spectrum | 6 |
| 4 | Results | 7 |
| 4.1 | UHECR fitted energy flux and resulting composition | 7 |
| 4.2 | Secondary neutrinos | 11 |
| 5 | Discussion | 11 |
| 6 | Conclusion | 14 |
| A | Simulation weighting | 15 |
| B | Relation between jet power and break energy | 16 |

1 Introduction

Ultra-high-energy cosmic rays (UHECRs), with energies exceeding $\sim 10^{18}$ eV, remain among the most challenging open problems in astrophysics. Although extensive measurements by the Pierre Auger Observatory and the Telescope Array have established the global features of the energy spectrum, mass composition, and arrival-direction distributions, the identification of the sources responsible for the highest-energy particles is still unresolved. Any viable model must simultaneously account for the observed spectral suppression at the highest energies, the energy-dependent evolution of mass-sensitive air-shower observables, and the anisotropies reported in arrival directions across angular and energy scales.

Radio galaxies have long been recognized as promising UHECR source candidates, as their relativistic jets and extended radio lobes provide large acceleration volumes, long activity timescales, and substantial kinetic power [1]. In particular, nearby FR-I radio galaxies combine favorable energetics with short propagation distances, thereby minimizing energy losses and making their potential contribution directly testable with current UHECR data. Among them, Centaurus A (Cen A), Virgo A (Vir A), and Fornax A (For A) stand out as the most prominent local systems, and they have been repeatedly discussed as benchmark sources in both theoretical and phenomenological studies.

Most previous investigations of radio galaxies as UHECR sources have relied on simplified assumptions for the injected particle spectrum, typically adopting a single power-law motivated by diffusive shock acceleration and treating source populations in a largely homogeneous manner [2–4]. In contrast, recent advances in the modeling of particle acceleration in

relativistic jets indicate that multiple acceleration mechanisms—including shock, shear, and stochastic processes—can operate simultaneously, leading to injection spectra with non-trivial shapes that deviate from simple power laws [5–8]. At the same time, growing observational evidence suggests that individual nearby sources may have undergone complex evolutionary histories, implying that source-specific properties can play a decisive role in shaping the observed UHECR flux.

The present work introduces a new, physically driven framework to test the role of nearby radio galaxies as UHECR sources. For the first time, we combine acceleration spectra derived from detailed jet-acceleration studies with source-specific properties of individual nearby FR-I radio galaxies, and we confront this framework directly with the UHECR energy spectrum measured by the Pierre Auger Observatory. Our approach departs from purely population-based treatments by modeling Cen A, Vir A, and For A individually, while simultaneously accounting for the cumulative contribution of the more distant radio galaxy population through a continuous distribution of sources. This hybrid strategy allows us to capture both the distinctive characteristics of the nearest sources and the unavoidable background from the broader radio-galaxy population.

A key strength of this work is the use of a minimal set of physically motivated parameters. Rather than fitting arbitrary injection spectra or compositions, we restrict our modeling choices to scenarios grounded in current theoretical and observational understanding of AGN jets, including acceleration efficiencies tied to jet power and composition scenarios motivated by astrophysical enrichment processes. Within this constrained framework, we determine the relative contribution of each nearby source and the background population by fitting exclusively to the measured UHECR energy spectrum. The resulting best-fit solutions then yield non-trivial predictions for the mass composition at Earth and for the associated flux of secondary neutrinos, providing additional, independent tests of the model.

By linking source-specific jet properties, realistic acceleration spectra, and full extragalactic propagation in a unified analysis, this study represents a significant step beyond previous phenomenological treatments of radio galaxies as UHECR sources. Our results demonstrate that a small number of well-motivated nearby radio galaxies, supplemented by a subdominant background population, can reproduce key features of the observed UHECR spectrum with physically reasonable acceleration efficiencies. In doing so, this work highlights the explanatory power of source-resolved modeling and establishes a robust framework for future multi-messenger tests of UHECR origin scenarios.

This paper is organized as follows. In Section 2 we describe the source emission models, including the adopted acceleration spectra, composition scenarios, and the treatment of individual and background radio galaxies. Section 3 details the extragalactic propagation setup and the statistical procedure used to fit the UHECR energy spectrum. The resulting source contributions, composition predictions, and neutrino fluxes are presented in Section 4. We discuss the physical implications of our findings in Section 5, and we summarize our conclusions in Section 6.

2 Radio galaxies as UHECR sources

In this section, we describe the properties we used for radio galaxies as potential sources of UHECRs. Our implementation considers details of a) the energy spectrum, b) the mass composition, c) the emitted power, and d) the source distribution in the Universe. We follow a two-pronged approach: the nearest and brightest sources are modeled individually

| RG | Distance (Mpc) | Q_{jet} (10^{43}erg s^{-1}) | R_{break} (EV) | Γ_{eff} |
|-------|----------------|---|-------------------------|-----------------------|
| Cen A | 3.8 | 2 [19] | 5.7 | 1.2 [20] |
| Vir A | 16.4 | 5 [21] | 8.2 | 2.5 [22] |
| For A | 20.8 | 0.24 [23] | 2.4 | 1.5 [24]* |

Table 1. Parameters for Centaurus A, Fornax A and Virgo A. * The value was estimated based on a class of sources with similar characteristics to Fornax A [25].

(Centaurus A, Fornax A and Virgo A), allowing us to account for their specific physical characteristics, while the remaining, more distant population of radio galaxies are treated statistically through a continuous distribution.

2.1 Energy spectrum and composition

We use two functional forms to describe the emitted energy spectrum of radio galaxies: a) power-law with exponential cutoff (PLEC) and b) a double power-law with exponential cutoff (DPLEC).

Canonical Fermi acceleration and subsequent developments [9–11] suggest that diffusive shock acceleration (DSA) results in an emitted energy spectrum given by a power-law suppressed by an exponential cutoff

$$\left(\frac{dN}{dE}\right)_{\text{PLEC}} = \left(\frac{E}{E_{\text{break}}}\right)^{-s} \exp\left(-\frac{E}{E_{\text{break}}}\right), \quad (2.1)$$

where the spectral index s is approximately $s = 2$ for non-relativistic shocks [12] and $s \approx 2.2 - 2.3$ for relativistic shocks [13]. The exponential cutoff accounts for the finite size and/or the finite acceleration power of the source.

The calculations done by Seo et al. [6] for FR-I radio galaxies considering multiple acceleration mechanisms such as DSA, turbulence, and shear acceleration in the jet and in the environment resulted in emitted energy spectrum described by a double power-law with an exponential cutoff

$$\left(\frac{dN}{dE}\right)_{\text{DPLEC}} = \left[\left(\frac{E}{E_{\text{break}}}\right)^{2.6} + \left(\frac{E}{E_{\text{break}}}\right)^{0.6}\right]^{-1} \exp\left(-\frac{E}{E_{\text{break}}\Gamma_{\text{eff}}^2}\right), \quad (2.2)$$

where E_{break} is the break energy of the power-law and Γ_{eff} is the mean Lorentz factor of the spine of the jet.

The break energy depends on the acceleration efficiency and escape, being approximately given by the Hillas energy for efficient acceleration models [6]. Motivated by the Hillas-Lovelace limit [14, 15], we estimate E_{break} as a function of the jet power Q_{jet} as can be seen in Appendix B). The same value of E_{break} can be assumed for PLEC and DPLEC energy spectrum.

Nongradual shear acceleration boosts the maximum energy achievable for particles by a factor Γ_{eff}^2 , in the so-called espresso acceleration [16]. For many AGNs, Γ_{eff} and Q_{jet} can be estimated from electromagnetic measurements [17, 18]. Table 1 shows Q_{jet} , R_{break} and Γ_{eff} for Centaurus A, Fornax A and Virgo A.

| Composition | f_H | f_{He} | f_N | f_{Si} | f_{Fe} |
|-------------|-------|----------|--------------------|--------------------|--------------------|
| Solar | 0.922 | 0.078 | 8×10^{-4} | 8×10^{-5} | 3×10^{-5} |
| Wolf-Rayet | 0 | 0.62 | 0.37 | 0.01 | 0 |

Table 2. Fraction of elements for *Solar* and *Wolf-Rayet* composition hypothesis.

The composition of UHECR emitted by a source is largely unknown. We consider two astrophysical motivated hypothesis: *Solar* and *Wolf-Rayet*. *Solar* is a light mass composition, where the abundance of elements is equal to the Solar System [26]. *Wolf-Rayet* consists of an intermediate mass composition, based on the abundance of elements in Wolf-Rayet stellar winds [4, 27, 28]. The abundance of each representative nucleus composition is presented in Table 2.

2.2 Emitted Power

Assuming that the cosmic ray acceleration occurs in the relativistic jet, the cosmic ray luminosity can be estimated as a fraction of the total power of the jet. The cosmic ray emission rate per energy unit was written as

$$\frac{dN_j}{dEdt} = \eta f_j \frac{Q_{\text{jet}}}{E_{\text{jet}}^{\text{cr}}} \left(\frac{dN}{dE} \right)_{\text{model}}, \quad (2.3)$$

where f_j is the fraction of nuclear species j at the source, Q_{jet} is the total jet kinetic power, and $0 \leq \eta \leq 1$ is the fraction of jet power converted to nonthermal cosmic rays. The normalization factor

$$E_{\text{jet}}^{\text{cr}} = f_H \int_{E_0}^{E^*} dEE \left(\frac{dN}{dE} \right)_{\text{DSA}} + \sum_j f_j \int_{E^*}^{\infty} dEE \left(\frac{dN}{dE} \right)_{\text{model}}, \quad (2.4)$$

accounts for the total energy in cosmic rays. The lower energy bound in the integral, E_0 , is adopted as $E_0 = Am_p c^2$. The upper limit is approximated as infinity due to the exponential cutoff.

Based on the acceleration timescales derived by Seo *et al.* [5], we assume that for energies below $E^* = 10^{17}$ eV, the spectrum will be dominated by the standard DSA mechanism with $s = 2$. Although the acceleration timescale for nongradual shear acceleration is shorter than that for DSA, the former is only operative when the scattering mean free path is large enough to cross the jet-backflow interface [5]. Since the composition content of AGN jets remains uncertain, we assume the hadronic component is largely dominated by protons for energies below E^* as a simplification [29].

2.3 Sources distribution

The most prominent individual candidates are the nearby FR-I radio galaxies Centaurus A (Cen A, NGC 5128, 3.8 Mpc), Virgo A (Vir A, M87, 16.4 Mpc), and Fornax A (For A, NGC 1316, 20.8 Mpc) [30–32]. These objects are widely recognized in the literature as the most promising local UHECR sources, owing to their favorable combination of substantial jet power and proximity to Earth [2, 33–36]. Their individual treatment is further motivated by their angular proximity to UHECR excesses reported by large-scale experiments, which has led several studies to investigate their potential contributions in detail [33, 37]. Nevertheless,

these three radio galaxies are not expected to be the sole contributors to the observed UHECR flux. We therefore also include, in our calculations, the cumulative background contribution from the more numerous and distant population of radio galaxies. In the following, we refer to Cen A, Vir A and For A as nearby sources and to the others as background contribution.

The background contribution was estimated using a continuous distribution of sources [2]. The UHECR emissivity was derived from the continuous source function $\Psi(E, z)$, expressed in terms of the radio luminosity L , energy E , and redshift z ,

$$\Psi_j(E, z) \equiv \frac{dN_j}{dV dE dt} = \int dL \frac{dN_{\text{RG}}}{dV dL}(L, z) \left[\frac{dN_j}{dE dt}(E, Q_{\text{jet}}(L)) \right], \quad (2.5)$$

for each nuclear species j with atomic number Z .

The first term in the equation 2.5 represents the number of radio galaxies per luminosity per volume, and is estimated through radio luminosity functions (RLFs). A recent updated RLF for local FRI radio galaxies (separately from FRII) with $z < 0.3$ was obtained by Jong *et al.* [38] as

$$\frac{dN_{\text{RG}}}{dV d \log L} = \rho_0 \left[\left(\frac{L_\nu}{\bar{L}} \right)^\alpha + \left(\frac{L_\nu}{\bar{L}} \right)^\beta \right]^{-1}, \quad (2.6)$$

with $\rho_0 = 10^{-5.5} \text{Mpc}^{-3} d \log L^{-1}$, $\alpha = 0.59$, $\beta = 2.0$, and $\bar{L} = 10^{25.8} \text{W Hz}^{-1}$. For higher redshifts, we use the straightforward evolution $\Psi_j(E, z) = \Psi_j(E, z = 0) \varepsilon(z)$ with $\varepsilon(z) \propto (1+z)^m$. Considering that, for medium-high luminosity AGNs, we take a piecewise evolution with $m = 5$ for $z < 1.7$, $m = 0$ for $1.7 < z < 2.7$, and $m = 2.7 - z$ for $z > 2.7$, following Refs. [39–41].

The second term in equation (2.5) is the energy spectrum injected by the source, as described in section 2.1. In the absence of specific parameters for each source, we approximate $\Gamma_{\text{eff}} \approx 2$ [42, 43] and use Appendix B to predict E_{break} from Q_{jet} . Using the empirical relation between jet power and the 151 MHz radio luminosity [44], eq. (2.5) is written in terms of Q_{jet} as

$$\Psi_j(E, z) = \frac{7}{6} \eta f_j \rho_0 \varepsilon(z) I(E), \quad (2.7)$$

with

$$I(E) = \int_{Q_{\text{jet}}^{\text{min}}}^{Q_{\text{jet}}^{\text{max}}} \frac{dQ_{\text{jet}}}{\left(\frac{Q_{\text{jet}}}{f^{3/2} \bar{Q}} \right)^{7\alpha/6} + \left(\frac{Q_{\text{jet}}}{f^{3/2} \bar{Q}} \right)^{7\beta/6}} \left[\frac{1}{E_{\text{jet}}^{\text{cr}}} \left(\frac{dN}{dE} \right)_{\text{model}} \right] \Big|_{(E, E_{\text{break}}(Q_{\text{jet}}))}, \quad (2.8)$$

where $(dN/dE)_{\text{model}}$ and $E_{\text{jet}}^{\text{cr}}$ are as defined in sections 2.1 and 2.2, f_j is the fraction of nucleus j in the composition, and $\bar{Q} \equiv Q_{\text{jet}}(\bar{L})/f^{3/2}$. The factor $1 \leq f \leq 20$ accounts for uncertainties in the conversion from radio luminosity to jet power. We adopt $f \sim 10$, which provides a reasonable order-of-magnitude estimate for FR-I radio galaxies [45].

The integration limits correspond to the least and most powerful radio galaxies considered. We set $(Q_{\text{min}}, Q_{\text{max}}) = (10^{43}, 2 \cdot 10^{46}) \text{erg s}^{-1}$ to be consistent with limits used by Jong *et al* [38]. Based on our numerical tests and the results from Eichmann *et al* [2], the observed UHECR flux depends only weakly on Q_{min} .

3 Simulation setup and data analysis method

3.1 Extragalactic propagation

The propagation of astroparticles through the extragalactic medium was simulated using the CRPropa3.2.1 [46] framework. We performed one-dimensional propagation in the absence of magnetic fields. The sources were simulated as emitting a power-law spectrum with spectral index -1 over the range $[E_{\min}, E_{\max}] = [10^{18}, 10^{21}]$ eV, providing a uniform number of events per energy decade. The injected composition included equal fractions of ^1H , ^4He , ^{14}N , ^{28}Si , and ^{56}Fe primaries. The energy spectra explained in section 2.1 are introduced later in the data analysis by weighting procedure explained in Appendix A.

CRPropa3.2.1 considers photo-pion production, photo-pair production, and photo-disintegration in UHECR propagation using the *Gilmore12* extragalactic background light model [47] and the cosmic microwave background as photon targets. Nuclei were also subject to nuclear decay. Finally, adiabatic energy losses due to the expansion of the Universe were taken into account for all particles. The cosmological parameters were $H_0 = 67.3 \text{ km s}^{-1} \text{ Mpc}^{-1}$, $\Omega_m = 0.315$, and $\Omega_\Lambda = 1 - \Omega_m$ [48]. Nuclei and neutrinos were discarded if their energies fall below 0.9 EeV and 0.1 PeV, respectively.

Cen A, Vir A and For A were simulated as point-source emitters. The background contribution was simulated as sources uniformly distributed in a region between D_{\min} and D_{\max} (1D shell-like). The comoving distances were logarithmically spaced from 25 Mpc out to 4 Gpc. The number of primary events simulated was $N = 10^6$ per point source and per shell. For further details, see Appendix A.

3.2 Procedure to fit the measured energy spectrum

Our model consists of four flux contributions: i) Cen A, ii) Vir A, iii) For A and iv) background. We fit our model to the energy spectrum measured by Pierre Auger Observatory [49] by searching for the set of fractions of each one of the four fluxes that best describes the data. Therefore, the fit parameters are the contribution of Cen A, Vir A, For A and background to the total flux measured by the Pierre Auger Observatory.

We used the CERN ROOT framework [50] along with Minuit2 minimizer. The fit procedure minimizes the deviance $D = -2 \ln(L/L_{\text{sat}})$, where L is the likelihood of our model and L_{sat} is the likelihood of a model that perfectly describes the data [51, 52]. We consider the likelihood function a product of Gaussian distributions for the energy bins in which Pierre Auger Observatory measured events and a negative Poisson log-likelihood for the energy bins in which upper limits are set. The deviance is then $D = \sum_i d_i$, where for each i -th energy bin,

$$d_i = \begin{cases} (J_i^{\text{obs}} - J_i^{\text{mod}})^2 / \sigma_i^2, & \text{if } i \text{ is a measurement;} \\ 2J_i^{\text{mod}} / J_i^{\text{un}} & \text{if } i \text{ is an upper limit.} \end{cases} \quad (3.1)$$

Here J_i^{obs} is the observed flux and J_i^{mod} is the sum of the flux contribution from Cen A, Vir A, For A and the background. The quantity σ_i^2 denotes the statistical variance of the data; in the case of asymmetric uncertainties, we adopt the larger value.

For bins with zero observed events (reported as 90% confidence level upper limits [49]), the Poisson deviance reduces to $d_i = 2\mu_i$. The expected counts are written as $\mu_i = J_i^{\text{mod}} / J_i^{\text{un}}$, where J_i^{un} is the flux corresponding to one event in that bin. For an energy bin of width ΔE_i and exposure \mathcal{E} , this quantity is

$$J_i^{\text{un}} = \frac{c_i}{\Delta E_i \mathcal{E}}, \quad (3.2)$$

where c_i is a correction factor [53]. The final goodness-of-fit statistic is the deviance per degree of freedom, D/ndf , where the number of degrees of freedom (ndf) is given by the number of fitted data points minus the number of fit parameters.

4 Results

4.1 UHECR fitted energy flux and resulting composition

The framework developed here enables the investigation of several key questions, including the relative contribution of nearby sources with respect to the background, the influence of primary composition, and the shape and characteristic parameters of the energy spectrum. To address these questions, we define different combinations of model parameters, referred to as Scenarios, as summarized in Table 3.

For each Scenario, the corresponding prediction of the mean logarithmic mass number $\langle \ln A \rangle$ obtained at Earth is shown in comparison with measurements from the Pierre Auger Observatory [54]. The reported values of $\langle \ln A \rangle$ correspond to the Auger data points shown in the figure and are derived from measurements of the depth of maximum of air-shower profiles, X_{max} [54, 55]. Their results depend on the choice of hadronic interaction model used in the analysis: QGSJet [56], EPOS [57] or Sibyll [58].

Our model predictions for $\langle \ln A \rangle$ are obtained by computing the mean logarithmic mass number from the resulting mass fractions at Earth. The model is fitted exclusively to the energy spectrum measured by the Pierre Auger Observatory; $\langle \ln A \rangle$ is computed only *a posteriori* from the best-fit source parameters, which determine the relative abundances of nuclei arriving at Earth, and is not included as a fit observable.

| Scenario | Energy spectrum | s | With continuous sources? | Fit range (EeV) |
|----------|-----------------|-----|--------------------------|-----------------|
| 1.a | DPLEC | - | No | 20 – 200 |
| 1.b | DPLEC | - | Yes | 20 – 200 |
| 2.a | PLEC | 2.0 | No | 5 – 200 |
| 2.b | PLEC | 2.0 | Yes | 5 – 200 |
| 3 | PLEC | 2.3 | Yes | 5 – 200 |

Table 3. Scenarios tested in this work.

For all Scenarios considered, our model could not describe the energy spectrum measured by the Pierre Auger Collaboration when the *Solar* composition was used. The fit for all Scenarios using *Solar* composition resulted in $D/\text{ndf} \sim 10 - 50$ and a mean logarithmic mass evolution very light and flat, inconsistent with data. See figure 1 where the Scenario 1. b with *Solar* is shown. Therefore, *Solar* were not further investigated in the Scenarios due to their inability to reproduce any of the relevant observables. In the next results, the *Wolf-Rayet* composition is assumed.

The best-fit parameter sets and the corresponding deviance values for each Scenario are presented in Table 4, together with the reference to their associated plots. The parameter η was introduced as the fraction of the jet power converted to nonthermal cosmic rays. However, the jet power is determined indirectly via methods that rely on different proxies, varying one to two orders of magnitude in some cases [59]. Furthermore, AGN present variability, meaning that the relevant activity to UHECR acceleration could have happened in the past [33, 60]. Deflection by coherent EGMF [35, 61] and galactic magnetic field [62] can cause suppression or amplification of the UHECR flux from a given source. Therefore,

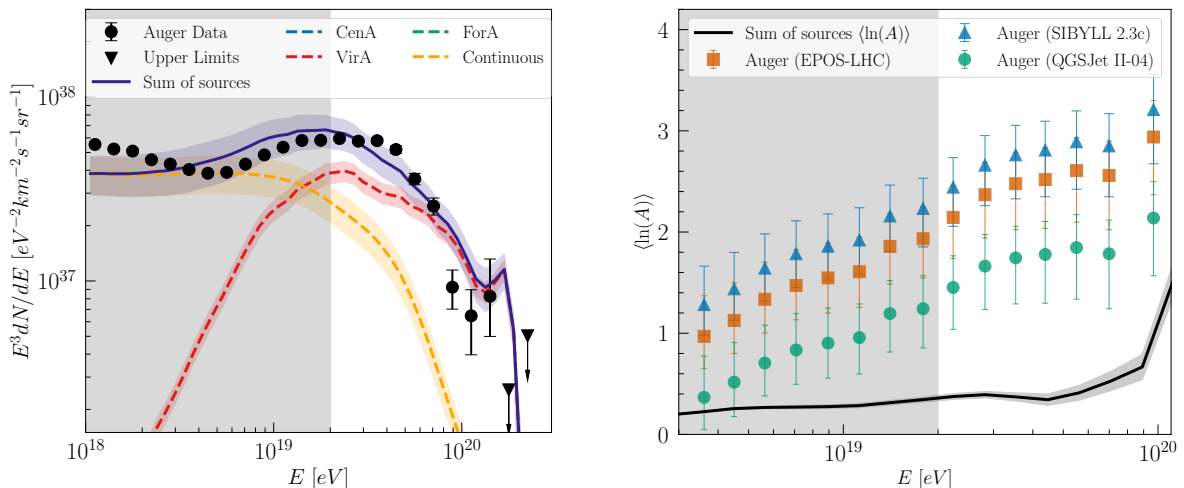


Figure 1. Results for Scenario 1.b using *Solar* composition. **Left:** Energy spectrum of UHECRs compared with the Pierre Auger Observatory data [49]. Contributions from individual nearby sources, a continuous source distribution (dashed yellow line) beyond the nearby radio galaxies and their sum are given respectively by dashed and solid lines with shaded bands (statistical uncertainties of the best-fit parameters). **Right:** Corresponding mean logarithmic mass number $\langle \ln A \rangle$ predicted by the summed source contribution (black solid line), compared with the Pierre Auger Observatory data [51] interpreted with different hadronic interaction models: EPOS-LHC, SIBYLL 2.3c and QGSJet II-04. Shaded vertical regions in both panels indicate energy ranges excluded from the fit.

| Scenario | Figure | $\eta_{\text{Cen A}}(10^{-3})$ | $\eta_{\text{Vir A}}(10^{-2})$ | $\eta_{\text{For A}}$ | $\eta_{\text{Cont}}(10^{-3})$ | D/ndf |
|----------|--------|--------------------------------|--------------------------------|-----------------------|-------------------------------|----------|
| 1.a | 2 | 3.7 ± 0.9 | 0 ± 20 | 5.4 ± 0.3 | - | 19.55/8 |
| 1.b | 3 | 6 ± 1 | 0 ± 2 | 3 ± 1 | 8 ± 3 | 6.16/7 |
| 2.a | 4 | 1.8 ± 0.1 | 0.00 ± 0.04 | 1.50 ± 0.04 | - | 84.52/14 |
| 2.b | 5 | 2.5 ± 0.2 | 0 ± 7 | 1.17 ± 0.07 | 0.25 ± 0.04 | 13.08/13 |
| 3 | 6 | 2.6 ± 0.7 | 1.3 ± 0.4 | 0.46 ± 0.05 | 0.00 ± 0.01 | 25.47/13 |

Table 4. Best-fit parameters for each Scenario.

since we are estimating η at the Earth, its interpretation is subject to these uncertainties. Although the values of η are expected to be closer when comparing different sources, the estimated values are likely to reflect these particularities.

Figures 2 to 6 present the energy spectrum fitted to the Pierre Auger Observatory data [49] and the respective $\langle \ln A \rangle$ for the studied Scenarios 3 considering the *Wolf-Rayet* composition. The shaded region indicates the energy range excluded from the fit therefore it should not be compared to the data.

Figure 2 shows the results for Scenario 1.a. For energies above 20 EeV, Scenario 1.a describes the data reasonably: $D/\text{ndf} = 19.55/8 = 2.44$. For A and Cen A produce the larger amount of the flux, while Vir A's contribution is negligible. The predicted evolution of $\langle \ln A \rangle$ with energy is consistent if EPOS-LHC and SIBYLL 2.3c interaction models are used.

Figure 3 shows the results for Scenario 1.b. This Scenario was proposed to investigate the influence of the background contribution in Scenario 1.a. The inclusion of background sources improves the description of the measured energy spectrum: $D/\text{ndf} = 6.16/7 = 0.87$.

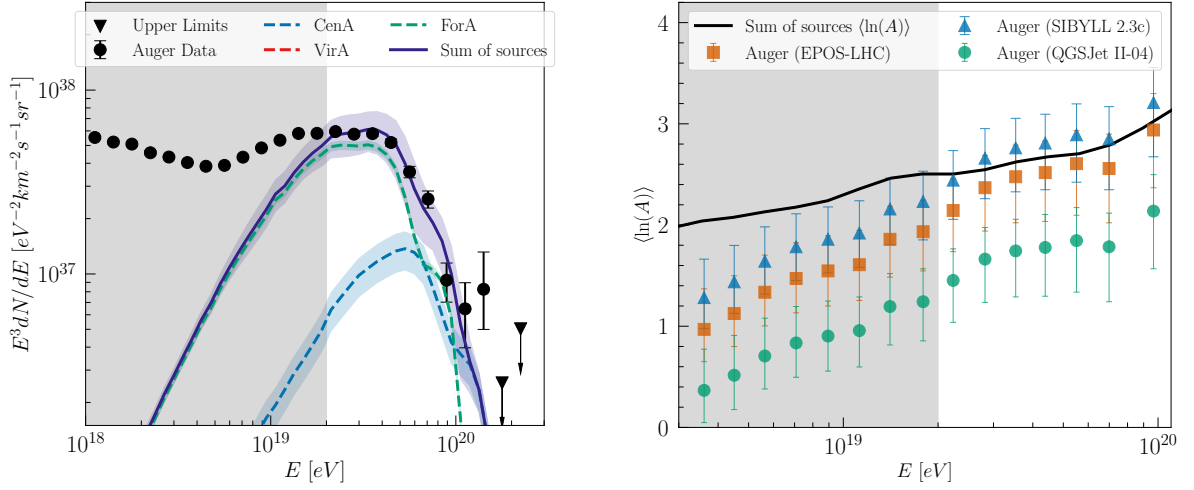


Figure 2. Resulting UHECR spectrum (left) and corresponding $\langle \ln A \rangle$ (right) for Scenario 1.a. The elements are the same as Figure 1, but without the continuous source distribution beyond the nearby radio galaxies.

The inclusion of more distant sources causes minor changes in parameters of the nearby sources to the measured flux. For A and Cen A have now similar contributions at Earth, and the flux from Vir A's remains negligible. The inclusion of distant sources improves the agreement between the predicted $\langle \ln A \rangle$ and the Auger data down to ~ 3 EeV, when compared with the results for Scenario 1.a.

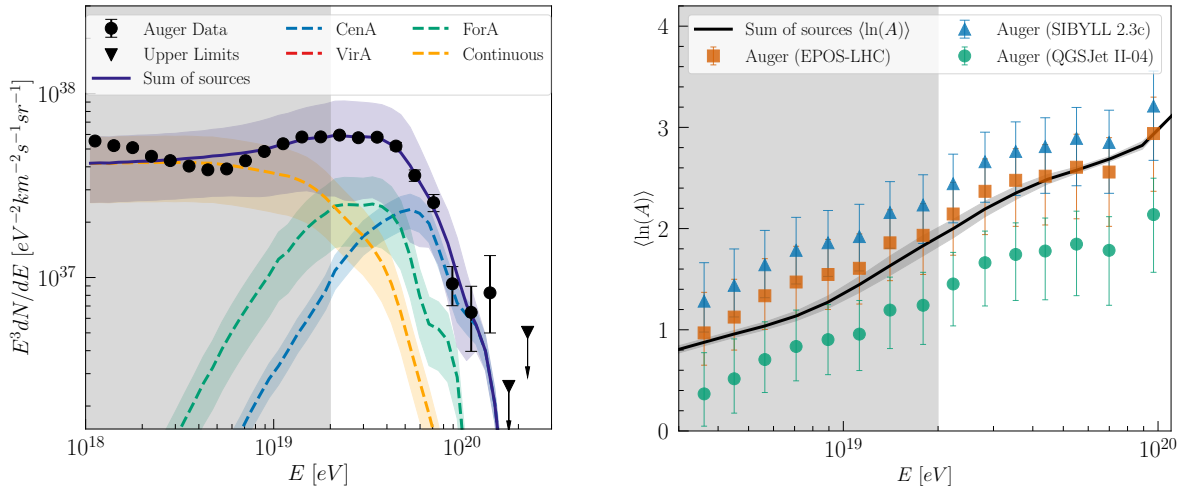


Figure 3. Resulting UHECR spectrum (left) and corresponding $\langle \ln A \rangle$ (right) for Scenario 1.b. The elements are the same as Figure 1.

Figures 4 and 5 present the results for Scenarios 2.a and 2.b, respectively. Scenarios 2.a and 2.b describe the data with less accuracy than Scenarios 1.a and 1.b, see D/ndf values in Table 4. However, note that the spectral index allows to expand the energy range where the

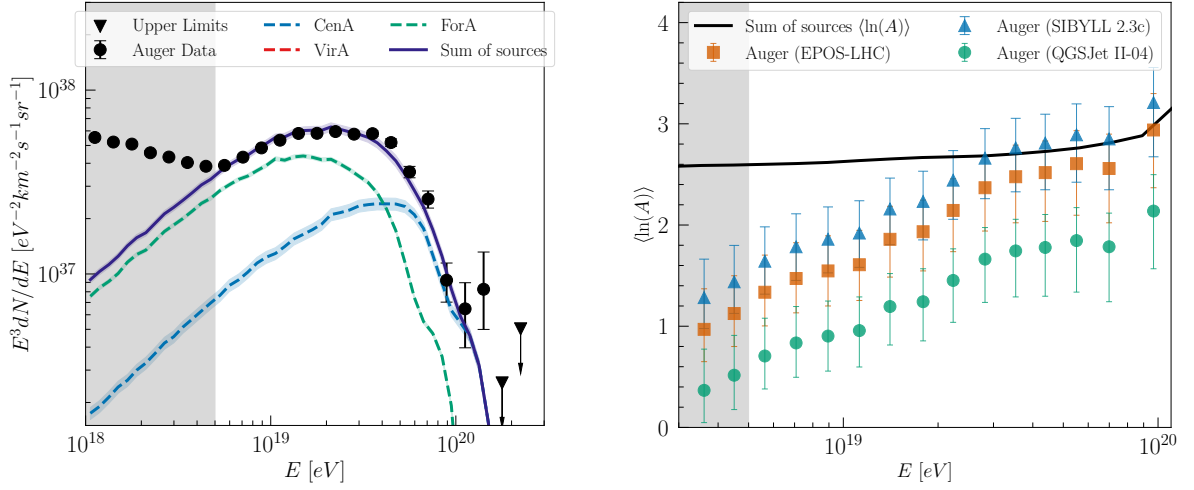


Figure 4. Resulting UHECR spectrum (left) and $\langle \ln(A) \rangle$ (right) for Scenario 2.a. The elements are the same as Figure 2.

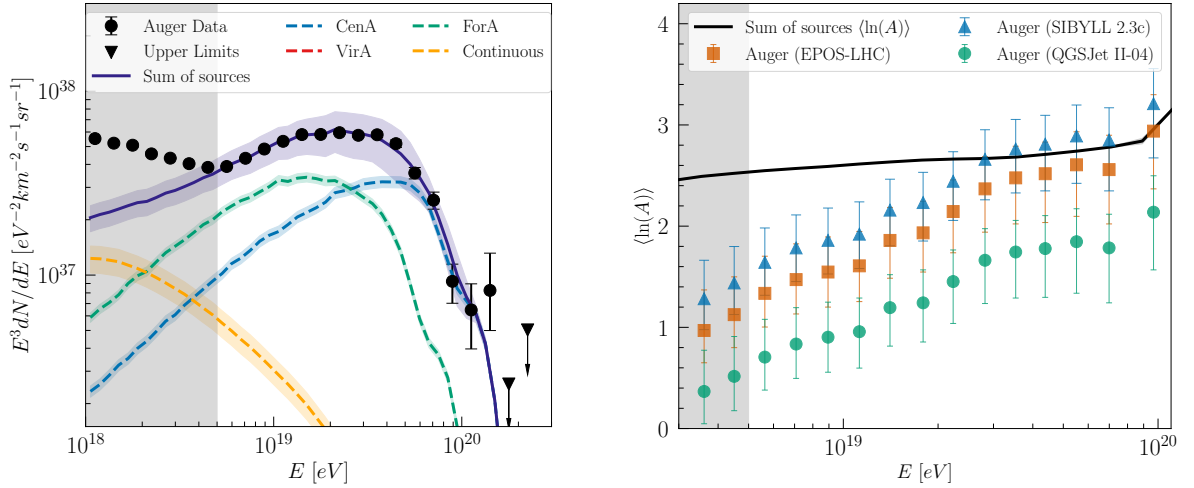


Figure 5. Resulting UHECR spectrum (left) and $\langle \ln(A) \rangle$ (right) for Scenario 2.b. The elements are the same as Figure 1.

fit is performed down to 5 EeV. As obtained for Scenarios 1.a and 1.b, the contribution of Vir A is negligible for both Scenarios 2.a and 2.b. The contribution of background sources to the total flux is smaller than Scenario 1.a and 1.b due to the extended energy cutoff of DPLEC (boosted by Γ_{eff}^2) and the extended fit range that provides additional limitations to η_{cont} . While Scenarios 1 reproduce the tendency of lighter mass when the energy decreases, in Scenarios 2 the mass evolution with energy is less steep and become clearly inconsistent with data for energies $\lesssim 20$ EeV.

Figure 6 show the results for Scenario 3 which was proposed to assess the importance of the spectral index of the injected flux. In this Scenario, Vir A emerges as a prominent source

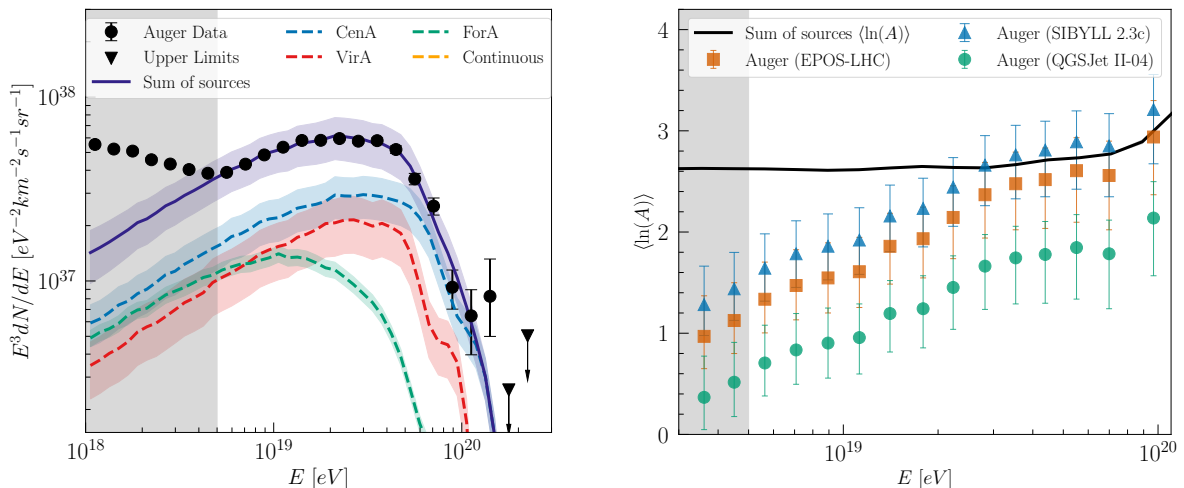


Figure 6. Resulting UHECR spectrum (left) and $\langle \ln(A) \rangle$ (right) for Scenario 3. The elements are the same as Figure 1.

and the background sources contribution to the total flux becomes negligible. This is the only Scenario in which $\eta_{\text{For A}} < 1$, although it remains two orders of magnitude higher than $\eta_{\text{Cen A}}$ and one higher than $\eta_{\text{Vir A}}$. On the other hand, $\eta_{\text{Cen A}}$ for Cen A continues consistent with the found in Scenarios 1 and 2. The mean logarithmic mass evolution with energy has the same flatness problem as seen in Scenarios 2.

4.2 Secondary neutrinos

The neutrinos produced by the interaction of the UHECR with the photon backgrounds were calculated for each Scenario. Figure 7 shows the flux of secondary neutrino for Scenarios 1.a and 2.a and figure 8 for Scenario 3 in comparison to the sensitivities of future experiments POEMMA [63], GRAND [64] and IceCube-Gen2 [65]. The flux of secondary neutrino from local sources is 3 – 4 orders of magnitude below the sensitivities of future experiments. The choice of the energy spectrum model has a minor effect on the predicted neutrino flux. The production of secondary neutrinos is highly sensitive to the composition given that lighter particles produce more neutrino [66, 67]. As the fraction of protons in the *Wolf-Rayet* composition is negligible, a very low flux of secondary neutrinos is produced.

Figure 9 shows the flux of secondary neutrinos for Scenarios 1.b and 2.b, in which background sources represent an important contribution to the flux measured at Earth. The neutrino yield depends on both the distance traveled by UHECRs and the number of contributing sources, both of which increase with distance. For the PLEC energy spectrum, the simulated neutrino flux exceeds the projected sensitivities of future experiments by a factor of approximately ~ 10 , raising the exciting possibility of detecting UHECR-induced neutrinos from distant AGNs in the near future.

5 Discussion

Table 5 presents the contribution of each source, for each Scenario, to the total flux measured by the Pierre Auger Observatory in the energy range over which the fits were performed.

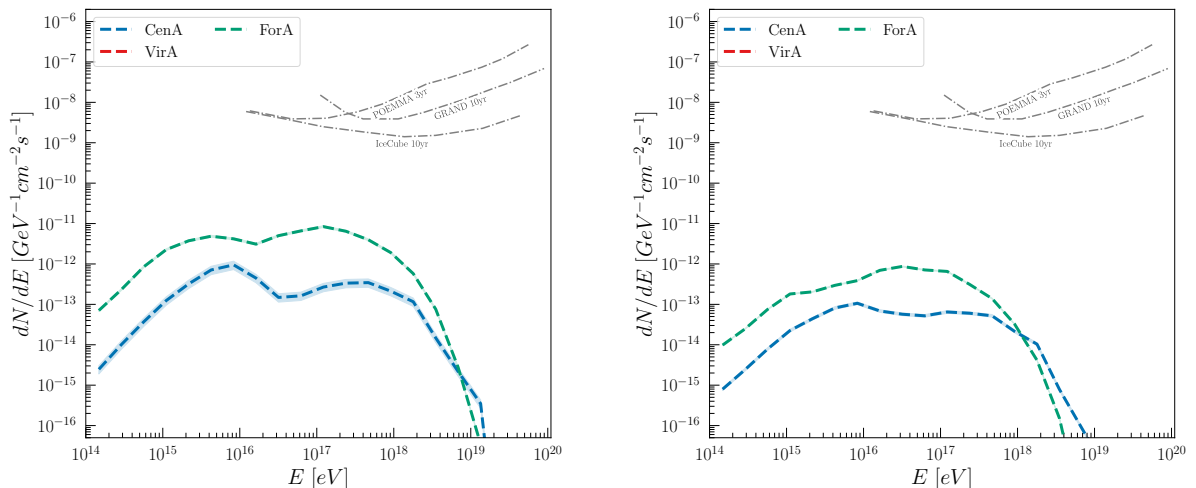


Figure 7. Flux of secondary neutrino for Scenarios 1.a (left) and 2.a. (right) compared with the sensitivities of future experiments POEMMA [63], GRAND [64] and IceCube-Gen2 [65]. The uncertainties are shown as a shaded band.

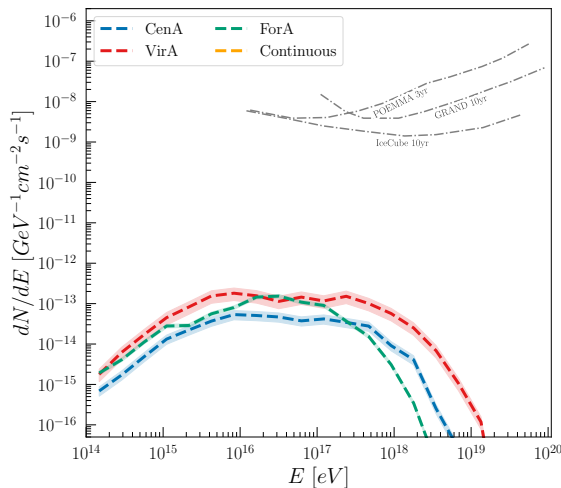


Figure 8. Flux of secondary neutrino for Scenario 3 compared with the sensitivities of future experiments POEMMA [63], GRAND [64] and IceCube-Gen2 [65]. The uncertainties are shown as a shaded band.

For the Scenarios considered, the total flux is largely dominated by local sources. The exact fraction of UHECRs originating from a given source, however, depends strongly on the assumed shape of the energy spectrum (PLEC or DPLEC), with the contribution from background sources remaining at the level of $\lesssim 20\%$.

Cen A dominance. Cen A exhibits a significant contribution across all Scenarios, with typical values of $\eta \sim 10^{-3}$. Owing to its proximity and current jet power, it consistently emerges as the dominant source of the UHECR flux in the Scenarios considered. This result is particularly compelling given that Cen A is located within a region where the Pierre Auger Observatory reports an excess of events above 60 EeV [68].

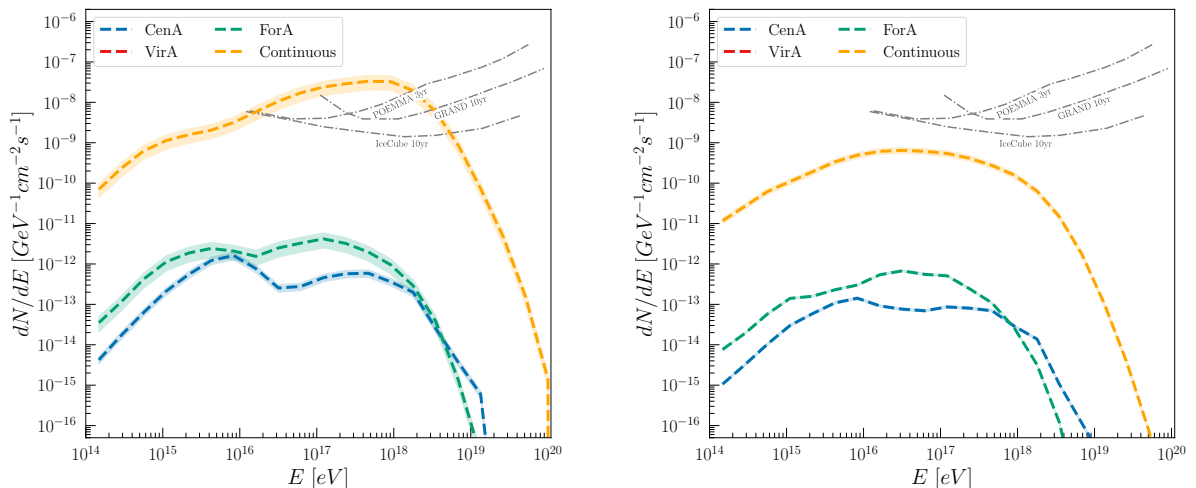


Figure 9. Flux of secondary neutrino for Scenarios 1.b. (left) and 2.b. (right) compared with the sensitivities of future experiments POEMMA [63], GRAND [64] and IceCube-Gen2 [65]. The uncertainties are shown as a shaded band.

| Scenario | Energy Range (EeV) | Cen A | Vir A | For A | Continuous |
|----------|--------------------|---------------|---------------|---------------|-----------------|
| 1.a | 20 – 200 | $30 \pm 7\%$ | $0 \pm 20\%$ | $66 \pm 3\%$ | - |
| 1.b | 20 – 200 | $51 \pm 11\%$ | $0 \pm 23\%$ | $33 \pm 13\%$ | $15 \pm 6\%$ |
| 2.a | 5 – 200 | $46 \pm 3\%$ | $0 \pm 1\%$ | $46 \pm 1\%$ | - |
| 2.b | 5 – 200 | $62 \pm 4\%$ | $0 \pm 19\%$ | $35 \pm 2\%$ | $1.6 \pm 0.3\%$ |
| 3 | 5 – 200 | $54 \pm 14\%$ | $31 \pm 11\%$ | $12 \pm 1\%$ | $0.0 \pm 0.1\%$ |

Table 5. Relative contribution of each source to the total flux measured by the Pierre Auger Observatory within the fit range.

The values of the parameter η (see Table 4) obtained for Cen A are consistent with those estimated by Matthews et al. [69], lying in the range $\sim 3 \times 10^{-3}$ to 5×10^{-2} , depending on the assumed spectral index (2.2–2.0). This agreement is particularly noteworthy, as in Matthews et al. the parameter η is inferred from physically motivated heuristic arguments, whereas in the present work it is derived directly from fits to the UHECR energy spectrum. If instead a relativistic shock spectrum with $s = 2.3$ is assumed, the resulting values of η are reduced by less than a factor of two, still remaining within the same order of magnitude.

For A past. Good description of the energy spectrum measured by the Pierre Auger Observatory was found for $\eta_{\text{For A}} > 1$. Aside from the discussed uncertainties in the jet power, these values are only achievable if For A presents a powerful past. In fact, For A exhibit some signs of higher activity in the past [25], and the necessity of it to explain the arrival directions of UHECRs was first pointed out by Matthews et al (2018) [33]. For A direction can be correlated with a region in which an excess of events above 40EeV was found in the Pierre Auger Observatory data [35, 68]. As the propagation times of UHECR are not equivalent to those for radio waves used as proxies for jet power measurements, particles could have undergone acceleration in a more extreme environment. To match the acceleration efficiency η found for other sources, For A should have been between 2 and 3 orders of magnitude more powerful in the past. However, the maximum energy can also be connected to the jet power.

This increase in Q_{jet} will shift E_{break} by factors $\sim 15 - 50$ (Eq. B.1). An alternative Scenario could be the magnetic amplification of the flux from For A, as obtained in de Oliveira & de Souza [61], however, only modest amplification factors (~ 2) were observed. A more likely explanation is related to time-delays imposed by the propagation of UHECR in the giant radio lobes [33, 60]. For A’s lobes extend to 122 – 170kpc, with an average magnetic field $\sim 3\mu\text{G}$ [25]. Comparing the results from [60] for Cen A (~ 200 kpc, $\sim 1 \mu\text{G}$), it is useful to get a qualitative picture. In this case, if For A presented a powerful past, UHECR with energies $\lesssim 30$ EeV may remain confined in the lobes for longer $\sim 0.1 - 1$ Myr, while more energetic $\sim 10^{20}$ eV escape more quickly. More final conclusions require a deeper study of the confinements of UHECR in the lobes of For A.

Vir A absence. Scenarios 1 and 2 result in a negligible contribution from Vir A to the total measured flux, whereas Scenario 3 predicts a substantial contribution from this source, amounting to $(31 \pm 10)\%$. This increase is driven by the change in the spectral index s of the injected energy spectrum. Larger values of s reduce the relative contribution of more distant sources, thereby forcing the fit to reproduce the observed flux predominantly through nearby sources, namely Cen A and Vir A.

Given its high jet power, it is unlikely that the jet of Vir A is incapable of accelerating UHECRs. Owing to its relative proximity, Vir A has long been advocated as a prominent contributor to the UHECR sky if active galactic nuclei are the dominant sources of these particles. For this reason, the persistent absence of an excess of UHECR events in the direction of Vir A, as reported by all UHECR experiments to date, has remained a puzzling feature for many years [31].

In this context, the lack of a detectable contribution from Vir A points toward the presence of a strong suppression mechanism acting on the UHECR flux emitted by this source. One possible explanation involves the structure of the extragalactic magnetic field (EGMF), which may significantly suppress or deflect the UHECR flux from Vir A. The galactic magnetic field (GMF) can also de-magnify its flux, as shown by Bister et. al. [62], with greater prominence for rigidities $\sim 1\text{EV}$. An alternative hypothesis is related to the internal structure of the source: cosmic-ray diffusion within the giant radio lobes of Vir A may be sufficiently slow to strongly limit the observable flux. Another plausible Scenario is that Vir A was less powerful in the past, at the epoch when UHECR acceleration would have occurred.

As discussed by Matthews et al. [33], the radio lobes of Vir A appear to be predominantly inflated by the current jet activity [70], in contrast to Cen A and For A, which show indications of a more violent past. In such a case, UHECRs originating from Vir A may not yet have had sufficient time to reach the Earth.

6 Conclusion

In this work, we presented a new, physically grounded framework to investigate the origin of ultra-high-energy cosmic rays (UHECRs) in nearby radio galaxies. By combining acceleration spectra derived from detailed modeling of particle acceleration in relativistic jets with numerical simulations of extragalactic propagation, we performed a source-resolved analysis of the three nearest FR-I radio galaxies—Centaurus A, Virgo A, and Fornax A—while consistently accounting for the cumulative contribution of the more distant radio-galaxy population.

A central result of this study is that the UHECR energy spectrum measured by the Pierre Auger Observatory can be reproduced with a minimal set of physically motivated

parameters. In the scenarios that best describe the data, the observed flux at the highest energies is largely dominated by nearby sources, with the background contribution remaining subdominant. The required acceleration efficiencies correspond to only a small fraction of the mechanical jet power, typically in the range $\eta \sim 10^{-3}$ – 10^{-2} , which is fully compatible with current theoretical expectations for particle acceleration in AGN jets.

Among the individual sources, Centaurus A consistently emerges as a major contributor across all viable Scenarios, in line with its proximity and jet power. Fornax A can also play a significant role, although the inferred efficiencies suggest that past activity or time-delay effects associated with particle confinement in extended radio lobes may be important. In contrast, Virgo A contributes negligibly in most Scenarios, and only becomes relevant for steeper injection spectra, reinforcing the long-standing puzzle posed by the absence of a clear UHECR excess from its direction.

The framework developed here also yields non-trivial predictions for the mass composition at Earth and for the associated flux of secondary neutrinos. While the model is fitted exclusively to the energy spectrum, the resulting composition trends are broadly consistent with observational constraints at the highest energies, and the predicted neutrino fluxes provide an additional, independent avenue for testing the scenario with future experiments.

Overall, this study demonstrates that a small number of nearby radio galaxies, modeled with realistic acceleration physics and supplemented by a subdominant background population, can account for key features of the observed UHECR spectrum. By moving beyond simplified injection assumptions and homogeneous source populations, our results highlight the importance of source-specific modeling in UHECR studies and establish a robust, predictive framework that can be further refined and tested with improved composition measurements, anisotropy studies, and next-generation multi-messenger observations.

A Simulation weighting

The simulation described in 3.1 were treated considering the weighting procedure to correct for inherent simulation biases and ensure the physical problem is treated correctly. For individual sources, each particle detected by the observer was assigned a weight that accounts for the emitted spectrum by the source and the source–Earth distance D . Accordingly, for each particle i detected by the observer we define

$$w^i = \frac{1}{4\pi D^2} \frac{dN_j}{dE dt} \frac{E_0^i \ln(10^3)}{N_j}, \quad (\text{A.1})$$

where N_j is the total number of injected particles of nuclear species j . The factor $E_0 \ln(10^3)$ results from the normalization of the injected spectrum, given by

$$\left[\frac{E_0^{-1}}{\int_{E_{\min}}^{E_{\max}} dE_0 E_0^{-1}} \right]^{-1} = E_0 \ln \left(\frac{E_{\max}}{E_{\min}} \right) = E_0 \ln(10^3). \quad (\text{A.2})$$

For continuous sources, the emission rate is obtained from the emissivity described in Section 2.3 and each shell k must be normalized by the injected particle density number $\rho^{-1} = (D_{\max} - D_{\min})/N_k$ in simulation. Hence, the weight is

$$w^i = \frac{1}{4} \frac{dN_j}{dV dt dE} E_0^i \ln(10^3) \frac{D_{\max} - D_{\min}}{N_k}, \quad (\text{A.3})$$

where the factor 1/4 accounts for the transition from the 1D to the 3D treatment.

B Relation between jet power and break energy

Seo *et al.* [5, 6] obtained E_{break} for several conditions, such as kinetic power, radius, and Lorentz factor of the jet. Based on the Hillas-Lovelace limit [14, 15], we expect a dominance dependence on the jet kinetic power, given by $E_{\text{break}} \propto Q_{\text{jet}}^{1/2}$. Figure 10 shows E_{break} as a function of Q_{jet} for the results in references [5, 6]. We estimate a general relation between the break energy and the kinetic power of the jet as

$$E_{\text{break}} = 4.3 \text{ EeV} \left(\frac{Q_{\text{jet}}}{10^{43} \text{ erg s}^{-1}} \right)^{0.41}. \quad (\text{B.1})$$

Note that the obtained dependence of E_{break} with Q_{jet} is weaker than predicted by the ideal Hillas-Lovelace limit, indicating a less efficient acceleration.

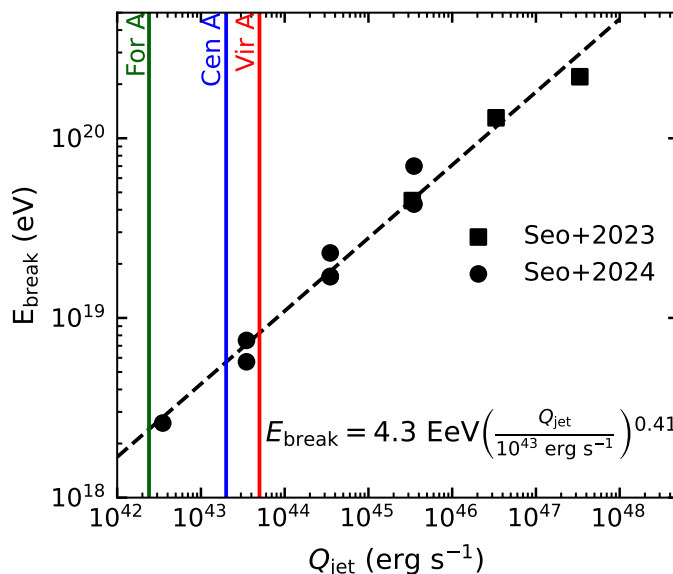


Figure 10. Relation of E_{break} and Q_{jet} for the data of Seo *et al.* (2023) [5] (squares) Seo *et al.* (2024) [6] (circles). The best fit is shown in a black dashed line. The estimated jet power for the nearby sources Cen A (blue), Vir A (red), and For A (green) is also shown.

Acknowledgments

The authors are supported by the São Paulo Research Foundation (FAPESP) through grant numbers 2021/01089-1, 2020/15453-4, 2024/22747-5, 2024/22722-2, 2024/22721-6, 2025/03325-5 and 2019/10151-2. VdS is supported by CNPq through grant number 308837/2023-1. The authors acknowledge the National Laboratory for Scientific Computing (LNCC/MCTI, Brazil) for providing HPC resources for the SDumont supercomputer (<http://sdumont.lncc.br>).

References

- [1] F.M. Rieger, *Active Galactic Nuclei as potential sources of Ultra-High Energy Cosmic Rays*, *Universe* **8** (2022) 607.

- [2] B. Eichmann, J. Rachen, L. Merten, A.v. Vliet and J.B. Tjus, *Ultra-High-Energy Cosmic Rays from radio galaxies*, *Journal of Cosmology and Astroparticle Physics* **2018** (2018) 036–036.
- [3] B. Eichmann, M. Kachelrieß and F. Oikonomou, *Explaining the UHECR spectrum, composition and large-scale anisotropies with radio galaxies*, *Journal of Cosmology and Astroparticle Physics* **2022** (2022) 006.
- [4] C. de Oliveira and V. de Souza, *Probing UHECR production in Centaurus A using secondary neutrinos and gamma-rays*, *The European Physical Journal C* **81** (2021) .
- [5] J. Seo, D. Ryu and H. Kang, *A simulation study of ultra-relativistic jets. III. particle acceleration in FR-II jets*, *The Astrophysical Journal* **944** (2023) 199.
- [6] J. Seo, D. Ryu and H. Kang, *Model spectrum of Ultrahigh-Energy Cosmic Rays accelerated in FR-I radio galaxy jets*, *The Astrophysical Journal* **962** (2024) 46.
- [7] L. Comisso, G.R. Farrar and M.S. Muzio, *Ultra-High-Energy Cosmic Rays accelerated by magnetically dominated turbulence*, *The Astrophysical Journal Letters* **977** (2024) L18.
- [8] R. Mbarek and D. Caprioli, *Bottom-up acceleration of Ultra-High-Energy Cosmic Rays in the jets of Active Galactic Nuclei*, *The Astrophysical Journal* **886** (2019) 8.
- [9] E. Fermi, *On the origin of the cosmic radiation*, *Phys. Rev.* **75** (1949) 1169.
- [10] A.R. Bell, *The Acceleration of cosmic rays in shock fronts. I*, *Mon. Not. Roy. Astron. Soc.* **182** (1978) 147.
- [11] R. Protheroe and T. Stanev, *Cut-offs and pile-ups in shock acceleration spectra*, *Astroparticle Physics* **10** (1999) 185.
- [12] M.S. Longair, *High Energy Astrophysics. Third Edition*, Cambridge University Press, United Kingdom (2011).
- [13] P.L. Biermann, E.-J. Ahn, P.P. Kronberg, G. Medina-Tanco and T. Stanev, *A possible nearby origin for the highest-energy events observed*, in *Physics and Astrophysics of Ultra-High-Energy Cosmic Rays*, p. 181–195, Springer (2002).
- [14] R.V.E. Lovelace, *Dynamo model of double radio sources*, *Nature* **262** (1976) 649.
- [15] A.M. Hillas, *The Origin of Ultra-High-Energy Cosmic Rays*, *Annual Review of Astronomy and Astrophysics* **22** (1984) 425.
- [16] D. Caprioli, *“Espresso” acceleration of Ultra-High-Energy Cosmic Rays*, *The Astrophysical Journal Letters* **811** (2015) L38.
- [17] E. Meyer, W. Sparks, M. Georganopoulos, R. Van der Marel, J. Anderson, S. Sohn et al., *Proper motions of jets on the kiloparsec scale: New results with HST*, *Galaxies* **5** (2017) 8.
- [18] L.E.H. Godfrey and S.S. Shabala, *Mutual distance dependence drives the observed jet-power–radio-luminosity scaling relations in radio galaxies*, *Mon. Not. R. Astron. Soc.* **456** (2016) 1172.
- [19] S.G. Neff, J.A. Eilek and F.N. Owen, *The complex north transition region of Centaurus A: Radio structure*, *The Astrophysical Journal* **802** (2015) 87.
- [20] B. Snios, S. Wykes, P.E.J. Nulsen, R.P. Kraft, E.T. Meyer, M. Birkinshaw et al., *Variability and proper motion of X-ray knots in the jet of Centaurus A*, *The Astrophysical Journal* **871** (2019) 248.
- [21] R. Anantua, A. Ricarte, G. Wong, R. Emami, R. Blandford, L. Oramas et al., *On the comparison of AGN with GRMHD simulations – II. M87*, *Monthly Notices of the Royal Astronomical Society* **528** (2023) 735
[\[https://academic.oup.com/mnras/article-pdf/528/1/735/56254238/stad3998.pdf\]](https://academic.oup.com/mnras/article-pdf/528/1/735/56254238/stad3998.pdf).

- [22] Mertens, F., Lobanov, A. P., Walker, R. C. and Hardee, P. E., *Kinematics of the jet in M 87 on scales of 100–1000 Schwarzschild radii*, *Astronomy & Astrophysics* **595** (2016) A54.
- [23] F.M. Maccagni, P. Serra, M. Gaspari, D. Kleiner, K. Morokuma-Matsui, T. Oosterloo et al., *AGN feeding and feedback in Fornax A—Kinematical analysis of the multi-phase ISM*, *Astronomy & Astrophysics* **656** (2021) A45.
- [24] L.M. Mullin and M.J. Hardcastle, *Bayesian inference of jet bulk-flow speeds in Fanaroff-Riley type II radio sources*, *Monthly Notices of the Royal Astronomical Society* **398** (2009) 1989–2004.
- [25] F. Maccagni, M. Murgia, P. Serra, F. Govoni, K. Morokuma-Matsui, D. Kleiner et al., *The flickering nuclear activity of Fornax A*, *Astronomy & Astrophysics* **634** (2020) A9.
- [26] B. Eichmann, *High energy cosmic rays from Fanaroff-Riley radio galaxies*, *Journal of Cosmology and Astroparticle Physics* **2019** (2019) 009–009.
- [27] R.-Y. Liu, X.-Y. Wang, W. Wang and A.M. Taylor, *On the excess of Ultra-High Energy Cosmic Rays in the direction of Centaurus A*, *The Astrophysical Journal* **755** (2012) 139.
- [28] A.L. Müller and A. Araudo, *Active Galactic Nuclei Metallicity Enrichment and UHECR Composition*, in *Proceedings of 7th International Symposium on Ultra High Energy Cosmic Rays — PoS(UHECR2024)*, vol. 484, p. 105, 2025, DOI.
- [29] A. Celotti and A.C. Fabian, *The kinetic power and luminosity of parsec-scale radio jets – an argument for heavy jets*, *Monthly Notices of the Royal Astronomical Society* **264** (1993) 228 [<https://academic.oup.com/mnras/article-pdf/264/1/228/3734484/mnras264-0228.pdf>].
- [30] G.L.H. Harris, M. Rejkuba and W.E. Harris, *The distance to NGC 5128 (Centaurus A)*, *Publications of the Astronomical Society of Australia* **27** (2010) 457–462.
- [31] O. Kobzar, B. Hnatyk, V. Marchenko and O. Sushchov, *Search for Ultra High-Energy Cosmic Rays from radiogalaxy Virgo A*, *Monthly Notices of the Royal Astronomical Society* (2018) .
- [32] M. Cantiello, A. Grado, J.P. Blakeslee, G. Raimondo, G. Di Rico, L. Limatola et al., *The distance to NGC 1316 (Fornax A): yet another curious case*, *Astronomy & Astrophysics* **552** (2013) A106.
- [33] J.H. Matthews, A.R. Bell, K.M. Blundell and A.T. Araudo, *Fornax A, Centaurus A, and other radio galaxies as sources of Ultrahigh Energy Cosmic Rays*, *Monthly Notices of the Royal Astronomical Society: Letters* **479** (2018) L76 [https://academic.oup.com/mnrasl/article-pdf/479/1/L76/56976831/mnrasl_479_1_l76.pdf].
- [34] R.G. Lang, A.M. Taylor, M. Ahlers and V. de Souza, *Revisiting the distance to the nearest ultrahigh energy cosmic ray source: Effects of extragalactic magnetic fields*, *Physical Review D* **102** (2020) .
- [35] C. de Oliveira and V. de Souza, *Nearby Active Galactic Nuclei and starburst galaxies as sources of the measured UHECRs anisotropy signal*, *Journal of Cosmology and Astroparticle Physics* **2023** (2023) 058.
- [36] P.L. Biermann and V. de Souza, *Centaurus A: The extragalactic source of cosmic rays with energies above the knee*, *The Astrophysical Journal* **746** (2012) 72.
- [37] S. Mollerach and E. Roulet, *Case for Centaurus A as the main source of Ultrahigh-Energy Cosmic Rays*, *Physical Review D* **110** (2024) .
- [38] de Jong, J. M. G. H. J., Röttgering, H. J. A., Kondapally, R., Mingo, B., van Weeren, R. J., Best, P. N. et al., *Cosmic evolution of FRI and FRII sources out to $z=2.5$* , *A&A* **683** (2024) A23.
- [39] R.A. Batista, R.M. de Almeida, B. Lago and K. Kotera, *Cosmogenic photon and neutrino fluxes in the Auger era*, *Journal of Cosmology and Astroparticle Physics* **2019** (2019) 002–002.

- [40] G.B. Gelmini, O. Kalashev and D.V. Semikoz, *Gamma-ray constraints on maximum cosmogenic neutrino fluxes and UHECR source evolution models*, *Journal of Cosmology and Astroparticle Physics* **2012** (2012) 044–044.
- [41] L. Ballo, F.J.H. Heras, X. Barcons and F.J. Carrera, *Exploring X-ray and radio emission of type 1 AGN up to $z \sim 2.3$* , *Astronomy & Astrophysics* **545** (2012) A66.
- [42] X.-H. Ye, X.-T. Zeng, D.-Y. Huang, Z. Zhang, Z.-Y. Pei and J.-H. Fan, *The beaming effect for Fermi-LAT-detected FR-I radio galaxies*, *Publications of the Astronomical Society of the Pacific* **135** (2023) 014101.
- [43] G.A. Verdoes Kleijn, S.A. Baum, P.T. de Zeeuw and C.P. O’Dea, *Core radio and optical emission in the nuclei of nearby FR I radio galaxies**, *The Astronomical Journal* **123** (2002) 1334.
- [44] C.J. Willott, S. Rawlings, K.M. Blundell and M. Lacy, *The emission line–radio correlation for radio sources using the 7C redshift survey*, *Monthly Notices of the Royal Astronomical Society* **309** (1999) 1017–1033.
- [45] X. Cao and S. Rawlings, *No evidence for a different accretion mode for all 3CR FR I radio galaxies*, *Monthly Notices of the Royal Astronomical Society* **349** (2004) 1419–1427.
- [46] R. Alves Batista, J. Becker Tjus, J. Dörner, A. Dundovic, B. Eichmann, A. Frie et al., *CRPropa 3.2 — an advanced framework for high-energy particle propagation in extragalactic and galactic spaces*, *Journal of Cosmology and Astroparticle Physics* **2022** (2022) 035.
- [47] R.C. Gilmore, R.S. Somerville, J.R. Primack and A. Domínguez, *Semi-analytic modelling of the extragalactic background light and consequences for extragalactic gamma-ray spectra*, *Monthly Notices of the Royal Astronomical Society* **422** (2012) 3189 [<https://academic.oup.com/mnras/article-pdf/422/4/3189/18601416/mnras0422-3189.pdf>].
- [48] K. Olive, *Review of particle physics*, *Chinese Physics C* **38** (2014) 090001.
- [49] THE PIERRE AUGER COLLABORATION collaboration, *Features of the energy spectrum of cosmic rays above 2.5×10^{18} eV using the Pierre Auger Observatory*, *Phys. Rev. Lett.* **125** (2020) 121106.
- [50] P. Canal, F. Rademakers, A. Naumann, S. Linev, O. Couet, L. Moneta et al., *ROOT-project/ROOT: v6-36-04*, Aug., 2025. 10.5281/zenodo.16944732.
- [51] A. Abdul Halim, P. Abreu, M. Aglietta, I. Allekotte, K. Almeida Cheminant, A. Almela et al., *Constraining the sources of Ultra-High-Energy Cosmic Rays across and above the ankle with the spectrum and composition data measured at the Pierre Auger Observatory*, *Journal of Cosmology and Astroparticle Physics* **2023** (2023) 024.
- [52] S. Baker and R.D. Cousins, *Clarification of the use of CHI-square and likelihood functions in fits to histograms*, *Nuclear Instruments and Methods in Physics Research* **221** (1984) 437.
- [53] A. Aab, P. Abreu, M. Aglietta, J.M. Albury, I. Allekotte, A. Almela et al., *Measurement of the cosmic-ray energy spectrum above 2.5×10^{18} eV using the Pierre Auger Observatory*, *Phys. Rev. D.* **102** (2020) .
- [54] THE PIERRE AUGER collaboration, *Measurement of the depth of maximum of air-shower profiles with energies between $10^{18.5}$ and 10^{20} eV using the surface detector of the Pierre Auger Observatory and deep learning*, *Phys. Rev. D* **111** (2025) 022003.
- [55] T.P.A. collaboration, A. Aab, P. Abreu, M. Aglietta, J. Albury, I. Allekotte et al., *Deep-learning based reconstruction of the shower maximum X_{max} using the water-Cherenkov detectors of the Pierre Auger Observatory*, *Journal of Instrumentation* **16** (2021) P07019.
- [56] S. Ostapchenko, *Monte Carlo treatment of hadronic interactions in enhanced Pomeron scheme: QGSJET-II model*, *Physical Review D* **83** (2011) .

- [57] T. Pierog, I. Karpenko, J.M. Katzy, E. Yatsenko and K. Werner, *EPOS LHC: Test of collective hadronization with data measured at the CERN Large Hadron Collider*, [*Physical Review C* **92** \(2015\)](#) .
- [58] F. Riehn, R. Engel, A. Fedynitch, T.K. Gaisser and T. Stanev, *Hadronic interaction model Sibyll 2.3d and extensive air showers*, [*Physical Review D* **102** \(2020\)](#) .
- [59] L. Foschini, B. Dalla Barba, M. Tornikoski, H. Andernach, P. Marziani, A.P. Marscher et al., *The power of relativistic jets: A comparative study*, [*Universe* **10** \(2024\)](#) .
- [60] C. de Oliveira and V. de Souza, *History of UHECR production in Centaurus A*, [*Monthly Notices of the Royal Astronomical Society* **545** \(2025\) staf2160](#).
- [61] C. de Oliveira and V. de Souza, *Magnetically induced anisotropies in the arrival directions of Ultra-High-Energy Cosmic Rays from nearby radio galaxies*, [*The Astrophysical Journal* **925** \(2022\) 42](#).
- [62] T. Bister, G.R. Farrar and M. Unger, *The large-scale anisotropy and flux (de)magnification of Ultrahigh-Energy Cosmic Rays in the galactic magnetic field*, [*The Astrophysical Journal Letters* **975** \(2024\) L21](#).
- [63] T.M. Venters, M.H. Reno, J.F. Krizmanic, L.A. Anchordoqui, C. Guépin and A.V. Olinto, *POEMMA’s target-of-opportunity sensitivity to cosmic neutrino transient sources*, [*Physical Review D* **102** \(2020\)](#) .
- [64] J. Álvarez Muñoz, R. Alves Batista, A. Balagopal V., J. Bolmont, M. Bustamante, W. Carvalho et al., *The giant radio array for neutrino detection (GRAND): Science and design*, [*Science China Physics, Mechanics & Astronomy* **63** \(2019\)](#) .
- [65] M.G. Aartsen, R. Abbasi, M. Ackermann, J. Adams, J.A. Aguilar, M. Ahlers et al., *IceCube-Gen2: the window to the extreme Universe*, [*Journal of Physics G: Nuclear and Particle Physics* **48** \(2021\) 060501](#).
- [66] D. Hooper, A. Taylor and S. Sarkar, *The impact of heavy nuclei on the cosmogenic neutrino flux*, [*Astroparticle Physics* **23** \(2005\) 11](#).
- [67] S. Chakraborty, P. Mehta and P. Sarmah, *A relook at the GZK Neutrino-Photon Connection: Impact of Extra-galactic Radio Background & UHECR properties*, [*Journal of Cosmology and Astroparticle Physics* **2024** \(2024\) 058 \[2307.15667\]](#).
- [68] P. Abreu, M. Aglietta, J.M. Albury, I. Allekotte, K. Almeida Cheminant, A. Almela et al., *Arrival directions of cosmic rays above 32 EeV from phase one of the Pierre Auger Observatory*, [*The Astrophysical Journal* **935** \(2022\) 170](#).
- [69] J.H. Matthews, A.R. Bell, K.M. Blundell and A.T. Araudo, *Ultrahigh Energy Cosmic Rays from shocks in the lobes of powerful radio galaxies*, [*Monthly Notices of the Royal Astronomical Society* **482** \(2018\) 4303–4321](#).
- [70] F.N. Owen, J.A. Eilek and N.E. Kassim, *M87 at 90 centimeters: A different picture*, [*The Astrophysical Journal* **543** \(2000\) 611](#).